Bioconjugate Chemistry

Article

Synthesis, Characterization and Selective Delivery of DARPin-Gold Nanoparticle Conjugates to Cancer Cells

Sergey Deyev, Galina Proshkina, Anastasiya Ryabova, Francesco Tavanti, Maria Cristina Menziani, Gennady Eidelshtein, Gabriel Avishai, and Alexander B. Kotlyar

Bioconjugate Chem., **Just Accepted Manuscript** • DOI: 10.1021/acs.bioconjchem.7b00410 • Publication Date (Web): 14 Aug 2017

Bioconjugate Chemistry is published by the American Chemical Society. 1155 Sixteenth Street N.W., Washington, DC 20036

Synthesis, Characterization and Selective Delivery of DARPin-Gold Nanoparticle Conjugates to Cancer Cells

Sergey Deyev[† ‡]*, *Galina Proshkina*[†], *Anastasiya Ryabova*[§], *Francesco Tavanti*[⊥], *Maria Cristina Menziani*[⊥], *Gennady Eidelshtein*[#], *Gabriel Avishai*[#], *Alexander Kotlyar*[#]*

[†]Shemyakin-Ovchinnikov Institute of Bioorganic Chemistry, Russian Academy of Sciences, Miklukho-Maklaya St, 16/10, Moscow 117997, Russia

[‡]National Research Tomsk Polytechnic University, 30 av. Lenina, Tomsk, 634050 Russia

[§]Prokhorov General Physics Institute, Russian Academy of Sciences, 38 Vavilova St, Moscow 119991, Russia

[⊥]Department of Chemical and Geological Sciences, University of Modena and Reggio Emilia, Via Campi 103, 41125 Modena, Italy

[#]Department of Biochemistry and Molecular Biology, George S. Wise Faculty of Life Sciences and the Center of Nanoscience and Nanotechnology, Tel Aviv University, Ramat Aviv, Tel Aviv 69978, Israel

KEYWORDS: DARPin, gold nanoparticles, tumor cells, molecular dynamics simulations.

ABSTRACT

We demonstrate that the designed ankyril repeat protein (DARPin) _9-29, which specifically targets human epidermal growth factor receptor 2 (HER 2), binds tightly to gold nanoparticles (GNPs). Binding of the protein strongly increases the colloidal stability of the particles. The results of experimental analysis and molecular dynamics simulations show that approximately 35 DARPin _9-29 molecules are bound to the surface of a 5 nm GNP and that the binding does not involve the receptor-binding domain of the protein. The confocal fluorescent

microscopy studies show that the DARPin-coated GNP conjugate specifically interacts with the surface of human cancer cells overexpressing epidermal growth factor receptor 2 (HER2) and enters the cells by endocytosis. The high stability under physiological conditions and high affinity to the receptors overexpressed by cancer cells make conjugates of plasmonic gold nanostructures with DARPin molecules promising candidates for cancer therapy.

INTRODUCTION

Cancer is one of the deadliest diseases. Efforts of many research laboratories worldwide are focused on specific targeting and elimination of cancer cells and tumors. At present, radiation and chemotherapy together with surgery are the most widely used treatment strategies employed to control and prevent different types of cancer. Despite a considerable success achieved in cancer prevention there is a great need for new methods and technologies that can ensure efficient and specific eradication of cancer cells without damaging healthy ones. Photothermal therapy (PTT) using nanoparticles is a promising approach for selective elimination of cancer cells [1-4]. Spherical gold particles strongly absorb light in the visible range and are capable to convert the energy of the absorbed light into heat. The amount of heat released by GNPs upon illumination[5] is sufficient to kill cancer cells in the vicinity of the nanoparticle. In order to be useful for PTT, the particles should be specifically delivered to pathological cells. One way to address this challenge is to functionalize the nanoparticles with tumor-specific targeting ligands that can be recognized by receptors overexpressed in cancer cells. Different proteins, such as growth factors, transferrin, and antibodies, were employed to specifically deliver nano-sized objects to pathological cells and tissues. [6-10] Binding of antibodies to nanoparticles in many cases leads to strong reduction of their specific affinity to antigens. This is mainly due to multiple orientations of antibody molecules on the surface of the nanoparticle and to distortion of the antibody's structure caused by interaction with the metal. [11, 12] Designed ankyril repeat proteins (DARPins), a novel class of non-IgG scaffolds based on naturally occurring ankyrin repeats,[13] circumvent the problems of complexity and instability and thus seem to be ideal ligands for targeting GNPs and other nano-objects to tumor-specific receptors. DARPins are small (13–20 kD), highly soluble in water, stable at different experimental conditions and characterized by very high affinity to their protein targets[13-16]. A set of DARPins that specifically bind to human epidermal growth factor receptor 2 (HER2) overexpressed in breast cancer and ovarian cells have been reported[14, 17]. It has been demonstrated recently[18-20] that conjugates between DARPins and toxic proteins can specifically bind to cells through interaction with the membrane-associated receptors and cause cell death. To the best of our knowledge, no data are available on interaction of noble metal nanoparticles with DARPins and on targeted delivery of the DARPin-nanoparticle conjugates to cancer cells.

Here we show that approximately 35 DARPin_9-29 molecules bind tightly to 5 nm GNPs. The protein coating layer protects the particles from aggregation; the DARPin-nanoparticle conjugates (DARPin-GNPs) are stable at high (up to 0.5 M) salt concentrations, in contrast to commonly used citrate-protected GNPs that completely and rapidly precipitate out of the solution at salt concentrations higher than 20 mM. DARPin-GNPs specifically bind to SK-BR-3 cells that overexpress receptor HER2 and are efficiently internalized into them by endocytosis.

RESULTS AND DISCUSSION

We have demonstrated that incubation of 5 nm (in diameter) GNPs with DARPin_9-29 yields stable DARPin-GNP conjugates that do not aggregate at relatively high (up to 0.5M) salt concentrations in contrast to the parent citrate-protected GNPs that precipitate out of the solution at salt concentrations higher than 20 mM. This is consistent with the formation of a protective protein layer on the surface of a nanoparticle[21-23]. The formation of the layer is supported by the AFM imaging analysis of the nanoparticles. As seen in Figure 1, the average diameter (corresponding to the height measured by AFM) of the DARPin-coated particles is greater by ~4 nm than that of the bare (non-coated) GNPs (see Figure 1).

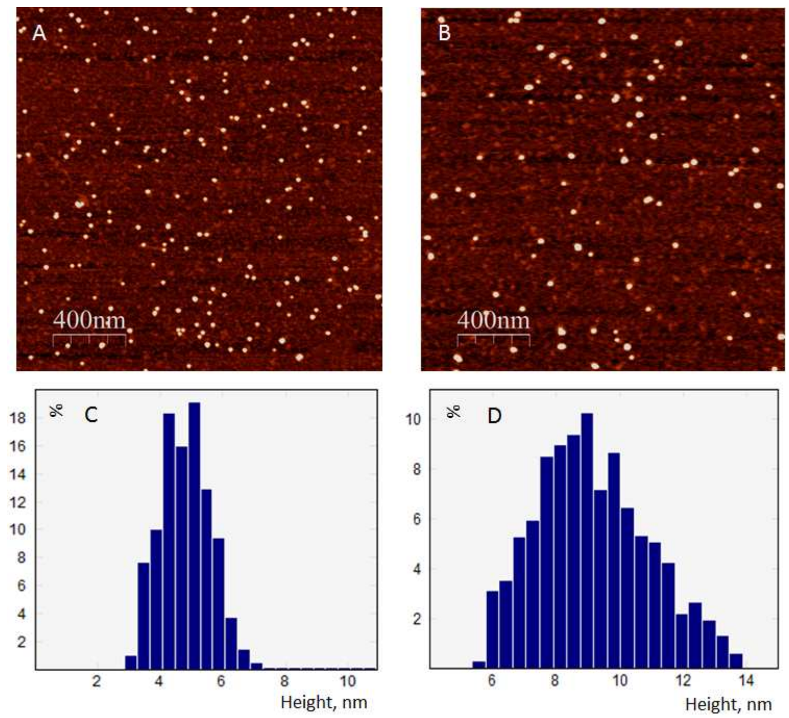

Figure. 1. AFM images (A, B) and statistical height analysis (C, D) of more than 1000 GNPs (A, C) and DARP-GNPs (B, D). The samples were deposited on a mica surface and imaged as described in Experimental Procedures. The average height (corresponding to diameter of GNPs) of DARPin-coated and bare GNPs are equal to 9.2 ± 1.8 and 4.9 ± 0.9 nm respectively ($n \geq 1000$).

The number of DARPin molecules bound to a particle was estimated spectrophotometrically using an extinction coefficient of 4.6×10^3 $M^{-1}cm^{-1}$ at 280 nm and 10^7 $M^{-1}cm^{-1}$at 520 nm for the DARPin and 5 nm (in diameter) GNPs, respectively. Contribution of the nanoparticle to the absorption of the conjugate at 280 nm is very high, making it impossible to determine the protein concentration. To quantify the protein content we have treated the conjugate with potassium cyanide. The treatment completely bleaches the absorption of the nanoparticles leaving the spectrum of the DARPin almost unaffected. The results of the spectral analysis (see Experimental Procedures for details) show that the DARPin to the GNP stoichiometry in the conjugate is approximately equal to 35.

Coarse-grained molecular dynamics (MD) simulations, carried out to study the interactions of DARPin proteins with GNPs at the molecular level, corroborate these results. Figure 2 shows the process of the protein corona formation during the simulation run. Fast protein adsorption

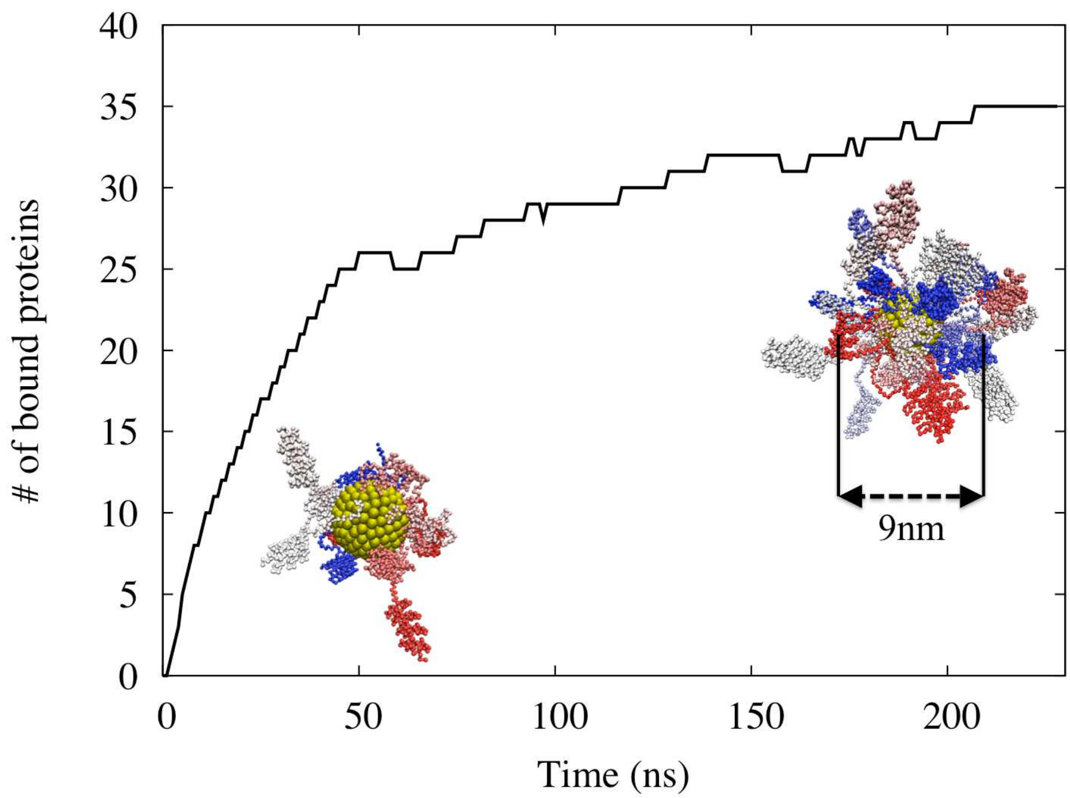

Figure. 2. Time evolution of the number of protein bound to the 5 nm GNP, and snapshots of the DARPin corona around GNP taken at 50 ns and 200 ns. Each protein is represented by different colour.

can be observed during the first 50 ns, then, the rate of adsorption slows down as the GNP surface becomes crowded. Finally a plateau corresponding to approximately 35 adsorbed protein molecules is obtained after 200 ns of simulation. The calculated diameter of the coated GNP is ~ 9±1nm. This result fits nicely with the diameter estimation by AFM (see Figure 1).

As seen in Figure 3 the DARPin molecules interact with the GNP through several domains, represented by the yellow spheres. Fortunately, the HER2 receptor-binding domain of the

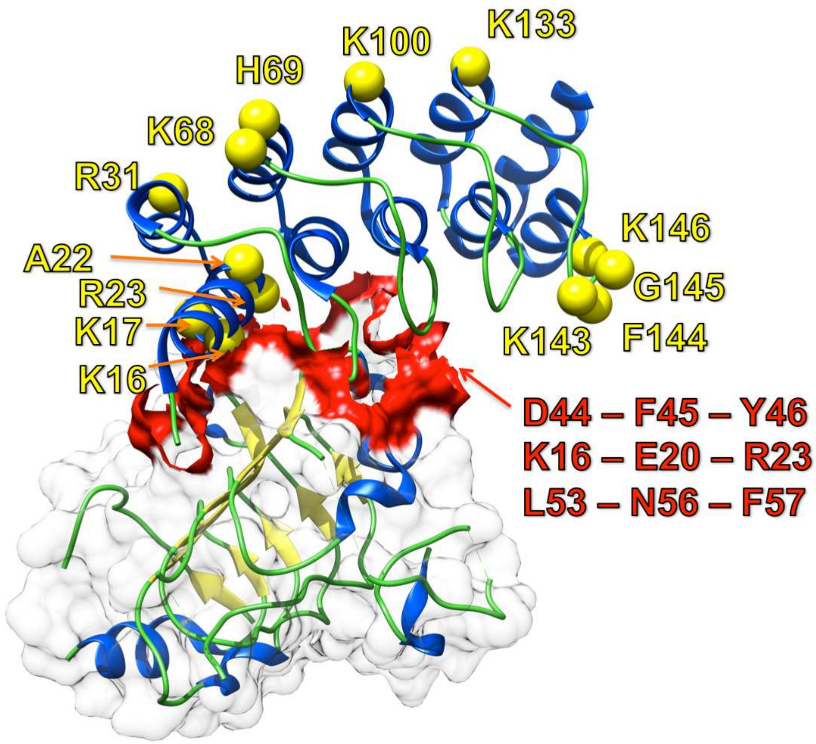

Figure. 3. Cartoon representation of DARPin_9-29 (top) docked to the HER2 (bottom). The DARPin molecule helices, sheets and coils are shown in blue, yellow and green respectively. The contact region between DARPin and HER2 is highlighted in red. Yellow spheres represent the DARPin regions, which are most probably involved in anchoring the protein to the GNP. The structure of the DARPin-HER2 complex[14] was retrieved from the RCSB PDB[28] (PDB ID: 4HRL).

DARPin is not involved in binding to the nanoparticle (see Figure 3). We thus expected that the binding affinity of the DARPin to HER2 will not be affected by interaction with the nanoparticle. The effect of the conjugates on adenocarcinoma cells (SK-BR-3) overexpressing HER2 demonstrated that this is indeed the case. Binding of the conjugate and its internalization into the cells was studied using fluorescent confocal microscopy. The DARPin-coated particles lacking fluorescence in the visible range of the absorption spectrum, were first labelled with FITC (DARPin-FITC-GNPs) as described in Experimental Procedures.

We have also used conjugates of the nanoparticles with the highly fluorescent hybrid protein, DARPin-m-Cherry (DARPin-m-Cherry-GNPs). We have shown that treatment of SK-BR-3 cells with either of the above conjugates at 4°C results in staining of the cell membranes (Figure 4, A and B); no fluorescence was detected either in the cytoplasm or in the nuclei. The staining is specific with respect to SK-BR-3 cells; CHO cells, lacking HER2 receptors show no fluorescence when treated under identical conditions (Figure 4, C and D). Treatment of

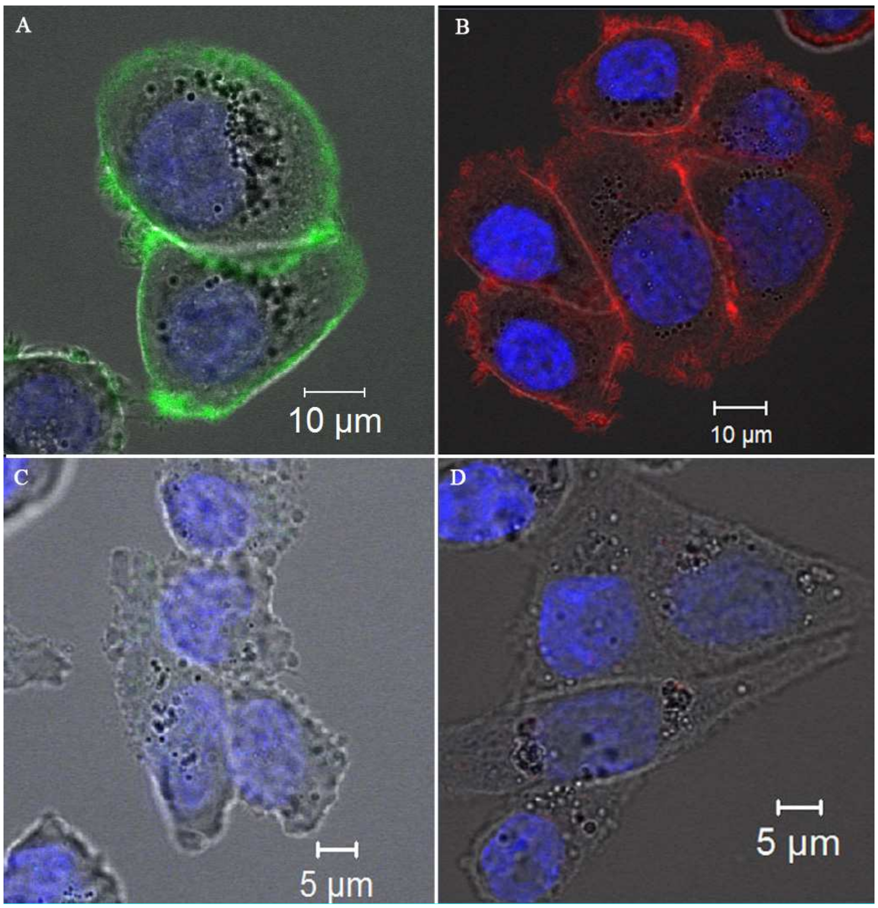

Figure 4. Specific interaction of DARPin-FITC-GNPs and DARPin-mCherry-GNPs with HER2 receptors on cell surface. SKBR-3 (A, B) and CHO (C, D) cells were incubated with DARPin-FITC-GNPs (A, C) or DARPin-mCherry-GNPs (B, D) at 4°C, as described in Experimental Procedures. Confocal fluorescent images of the cells were acquired at excitation wavelengths of 488 (A, C) or 561 nm (B, D). Superimposed images of the cells in blue-green and blue-red fluorescence channels are presented in panels A, C and B, D respectively. Nuclei were stained with Hoechst 33342.

SK-BR-3 cells with DARPin-FITC-GNP and DARPin-m-Cherry-GNP conjugates at 37°C leads to the appearance (in tens of minutes) of bright green and red fluorescent spots in the cytoplasm, respectively (see Figure 5, A and B). The kinetics of the internalization process

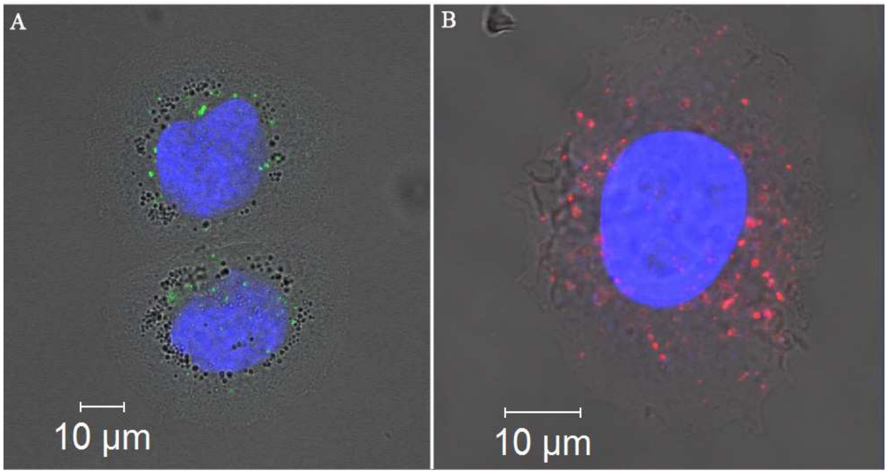

Figure 5. Specific internalization of DARPin-FITC-GNPs and DARPin-mCherry-GNPs by SKBR-3 cells at 37°C. The cells were treated with DARPin-FITC-GNPs (A) or DARPin-mCherry-GNPs (B) at 37°C as described in Experimental Procedures. Confocal fluorescent images of the cells were acquired at excitation wavelengths of 488 (A) or 561 nm (B). The picture presents superimposed images of the cells in blue-green (A) and blue-red (B) channels. Nuclei were stained with Hoechst 33342.

was studied by monitoring the time course of DARPin-FITC-GNPs appearance in different cell compartments. This was done by co-staining the conjugate with endosomal and lysosomal markers (see Figure 6). Yellow/orange spots in the images correspond to the conjugate located in either endosomes (Figure 6, A and D) or lysosomes (Figure 6, B and E). As evident from the data presented in Figure 6 the conjugate appears in early endosomes 10 min after beginning of the incubation. Accumulation of the conjugate in lysosomes takes about an hour. These results are consistent with internalization of the conjugate into the cell by receptor-mediated (energy-dependent) endocytosis mechanism.

CONCLUSIONS

We have demonstrated that incubation of citrate-protected GNPs with DARPin_9-29 yields very stable particles that resist high (up to 0.5 M) salt concentrations and do not aggregate

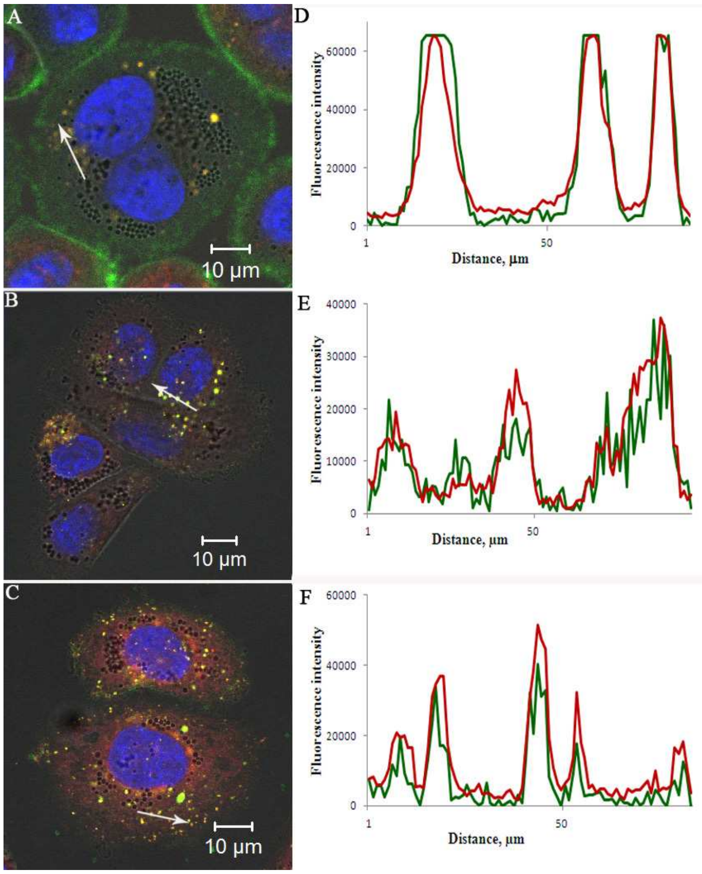

Figure 6. Internalization of DARPin-FITC-GNPs by SKBR-3 cells. The cells were incubated with 0.1 µM DARPin-FITC-GNPs. The unbound conjugates were washed away and the cells were subsequently incubated for 10 min (A), 1 h (B), or 2 h (C) at 37°C (see Experimental Procedures). The cells were further treated with Hoechst33342 and LysoTracker to stain the nucleus or lysosomes respectively. For early endosomes staining (A) the cells were treated with BacMan 2.0 a day before the experiment. Fluorescence intensity profiles along white arrows in A, B and C are shown on panels D, E and F, respectively. Green curves in D, E and F correspond to the fluorescence intensity profiles of DARPin-FITC-GNPs and red curves to the fluorescence intensity profiles of the organelle dyes.

under physiological conditions. The experimental results and the results of MD simulations (Figure 2) show that as many as 35 DARPin_9-29 molecules are connected to the nanoparticle. The diameter of the nanoparticle increases from 5 to 9 nm upon coating with the DARPin as evident the AFM analysis (Figure 1) and MD simulations (Figure 2). The thick protein layer surrounding the nanoparticle is responsible for high colloidal stability of the conjugate at high salt concentrations.

In many cases binding to nanoparticles leads to a significant reduction of affinity of tumor-targeting proteins, such as monoclonal antibodies or their fragments, to the receptors. [11,12] We have shown that this is not the case for DARPin_9-29. The results of calculations showed that the HER2-binding domain of the protein is not involved in binding to the nanoparticle (see Figure 2). The DARPin-GNP conjugate strongly and specifically binds to the surface of HER2-positive cells (Figure 4, A and B) and rapidly (in minutes) enters them by endocytosis (Figure 5). The high stability under physiological conditions and high affinity to the receptors overexpressed by cancer cells make conjugates of plasmonic gold nanostructures with DARPin molecules promising candidates for cancer therapy.

EXPERIMENTAL PROCEDURES

Unless otherwise stated reagents and chemicals were obtained from Sigma-Aldrich (USA) and were used without further purification.

Synthesis of GNPs. The citrate-protected 5 nm spherical gold nanoparticles were prepared by $HAuCl_4$ reduction with BH_4 essentially as described in. [24] The diameter of the nanoparticles estimated by TEM analysis was equal to 5.05±1 nm. Concentration of the particles was calculated using an extinction coefficient of $\sim 1 \times 10^7$ M^{-1} cm^{-1}at 520 nm. [25, 26].

Preparation of DARPin and DARPin-m-Cherry. E. coli BL21(DE3) strain was transformed with plasmids pDARPin-9_29 or pDARPin-9_29 –mCherry. [27] Fresh transformants (one colony per mL) were inoculated in 50 mL of the medium containing: 1% yeast extract, 1% triptone, 25 mM Na_2HPO_4, 25 mM KH_2PO_4, 100 mM NaCl, 2 mM $MgCl_2$ and 0.1 g/L ampicillin and grown at 37ºC with vigorous aeration. At a midlog phase (OD at 600 nm ~ 0.5) the incubation temperature was lowered to 28°C and isopropyl-thiogalactopyranoside was added to a final concentration of 1 mM. After induction for 8 h, the cells were harvested by centrifugation at 6000 g for 10 min at 4°C. The pellet was resuspended in a lysis buffer (500 mM NaCl, 20 mM Na-Pi, 30 mM imidazole, 0.5 mg/mL lysozyme, pH 7.5) and sonicated on ice. Cellular debris was removed by centrifugation at

15000 g; the supernatant was passed through a 0.22-μm filter and applied to a Ni^{2+}-NTA column (GE Healthcare, USA) equilibrated with 20 mM Na-Pi (pH 7.5), 500 mM NaCl, and 30 mM imidazole. DARPin was eluted by a linear gradient of imidazole (from 30 to 500 mM). The eluted protein was passed through Sephadex G-25 column (15 × 80 mm) equilibrated with 10 mM K-Pi (pH 7.5). The yields of purified DARPin-9_29 and DARPin-9_29-mCherry were approximately equal to 60 and 40 mg per liter of the growth medium respectively.

Coating of GNPs with DARPin and DARPin-m-Cherry. GNPs (2 μM; absorption ~20 at 520 nm) were incubated with 1 mg/mL of pDARPin-9_29 or 3 mg/mL DARPin-9_29-m-Cherry in 10 mM K-Pi buffer (pH 7.5) for 20 h. The incubation yielded stable nanoparticles that do not aggregate at relatively high (up to 0.5 M) salt concentrations in contrast to the parent nanoparticles that precipitate out of the solution at salt concentrations above 20 mM. The unbound protein was separated from the particles by size-exclusion chromatography on a Sepharose 4B column (1×16 cm) equilibrated in 10 mM K-Pi (pH 7.5). The conjugate was eluted in the void volume of the column, while the DARPin was eluted in the total volume.

For visualization by confocal microscopy, the DARPin-GNP conjugate lacking visible fluorescence was labeled with FITC as follows. The conjugate (absorption at 520 nm ~ 10) was incubated with 100 μM FITC for 40 h in 20 mM K-Pi (pH 7.5). The unbound dye was separated from the conjugate on a Sephadex G-25 column (15 × 80 mm) equilibrated with 10 mM K-Pi (pH 7.5). The void volume fraction was collected, left at 20°C for 16 h, and repeatedly passed through the same column. This procedure ensured a complete removal of non-bound FITC from the conjugates.

Estimation of DARPin to GNP ratio in the conjugate. Concentration of the GNPs was estimated using an extinction coefficient of 10^7 $M^{-1}cm^{-1}$ at 520 nm. Estimation of the protein content in the conjugate by absorption spectroscopy is challenging since the nanoparticle contributes very strongly to the absorbance of the conjugate at 280 nm. To make the estimation possible, we decomposed the GNP core in the conjugate by treatment with cyanide.

Cyanide etching leads to complete bleaching of the conjugate. The $Au(CN)^{2-}$ complex formed during the reaction was removed from the sample by extensive dialysis against 10 mM K-Pi (pH 7.5). Concentration of the protein was estimated using an extinction coefficient of 4.6×10^3 $M^{-1}cm^{-1}$ at 280 nm. The protein concentration in the sample exceeded the GNP concentration ~ 35 times. Similar result was obtained by computational analysis of the conjugate using MD simulations, as described below.

Molecular Dynamics Simulations. The structure of the DARPin - HER2 complex[14] was retrieved from the RCSB PDB[28] (PDB ID: 4HRL). The process of corona formation on the GNP was simulated by the coarse grained MD protocol previously developed by Tavanti et al[29,30]. The 5 nm (in diameter) GNP covered with citrates was modeled by 194 beads each carrying a negative charge (-3) placed uniformly at a distance of 2.5 nm from the neutrally charged central bead[31]. A repulsive potential described as a hard spherical wall with a radius of 25Å was assigned to the central bead in order to avoid penetration of the GNP by citrate and protein residues. The protein was modeled using a coarse-grained model where each amino acid is replaced by a single bead located on the α-carbon[32,33]. The Force Field for protein is described in.[29,30]

Molecular dynamics simulations were performed using the DL_POLY_2.20 package.[34] The system was first equilibrated at increasing temperatures, from 10 to 310 K with steps of 50 K; the temperature was controlled by a Berendsen thermostat with a coupling time of 1fs. Then three independent production runs at 310 K were performed for 500 ns by changing the initial velocities and using a stochastic thermostat with coupling time of 1fs.

Cell cultures. Cell lines SKBR-3 (human breast adenocarcinoma, ATCC number HTB-30), and CHO-K1 (Chinese hamster ovary, ATCC number CCL-61) were cultured in complete McCoy's 5A medium with 10% (v/v) heat-inactivated fetal calf serum (Thermo Scientific), 100 U/mL penicillin/streptomycin (Paneco) and 2 mM L-glutamine in a humidified incubator with 5% CO_2 at 37°C.

Confocal microscopy. SKBR-3 and CHO cells were cultured on glass bottom dishes (WillCo Well) overnight in 5% CO_2 at 37°C.

Binding of DARPin-FITC-GNPs and the DARPin-mCherry-GNPs to cell membranes was studied as follows. The cells were incubated in growth medium containing 0.1 μM of either of the above conjugates for 10 min at 4°C. The conjugates were washed away with the medium and the cells were visualized using a laser scanning microscope (Zeiss LSM-710-NLO).

Internalization of the conjugates into the cell organelles was conducted as follows. SKBR-3 and CHO cells were incubated in a growth medium containing: 100 nM DARPin-FITC-GNPs for 7 min at 37°C. The cells were washed twice with the medium and incubated in the fresh one for 1, 2 and 3 h at 37°C. For early endosome visualization, the cells were transduced with Cell Light Early Endosomes-RFP, BacMam 2.0 (Thermo Fisher, USA) in accordance with the manufacturer's instructions. For visualization of lysosomes, the cells were incubated with 50 nM LysoTrackerRed (Invitrogen) for 20 min at 37°C. The nuclei were stained with 2 nM Hoechst 33342 for 10 min at 37°C. The cells were finally washed twice with the medium and visualized using a laser scanning microscope (Zeiss LSM-710-NLO, Germany). DARPin-FITC-GNP conjugates were excited at 488 nm; the emission was recorded at 497–562 nm. LysoTrackerRed, Cell Light Early Endosomes-RFP and DARPin-mCherry-GNPs were excited at 561 nm; the emission was recorded at 566–683 nm. Hoechst was exited at 700 nm using femtosecond laser and the emission was detected at 400–600 mn. The 63× oil Plan-Apochromat objective with numerical aperture of 1.4 was used in order to obtain high-quality images.

Atomic Force Microscopy. AFM was performed on molecules adsorbed on muscovite mica. 100 μL of GNPs and DARPin-GNPs (absorbance ~0.01 at 520 nm) in 1 mM Mg-acetate were deposited on a freshly cleaved 1×1 cm mica plate; 5 min later the surface was rinsed with ultra-pure distilled water and dried by blowing nitrogen gas. AFM imaging was performed on a Solver PRO AFM system (NT-MDT, Russia), in a semi-contact (tapping) mode, using Si-gold-coated cantilevers (NT-MDT, Russia) with resonance frequency of 80–110 kHz. The images were "flattened" (each line of the image was fitted to a second-order polynomial, and the polynomial was then subtracted from the image line) by the Nova image processing software (NT-MDT, Russia). The images were analyzed and visualized using imaging software WSXM (Nanotec Electronica S.L., Madrid, Spain)[35].

ACKNOWLEDGEMENTS

This work was supported by the Israel Science Foundation, no. 1589/14, by the Russian Science Foundation (project no.14-24-00106), and by the Far2015 Unimore project.

AUTHOR INFORMATION

Corresponding Authors

*E-mail: s2shak@post.tau.ac.il

*E-mail: biomem@mail.ru

ORCID

Alexander Kotlyar: 0000-0003-0713-6499

Author Contributions

All authors contributed equally to this work.

Funding resources

The Israel Science Foundation and the Russian Science Foundation and the Italian Ministry of Education and Research.

Notes

The authors declare no competing financial interest.

ABBREVIATIONS

DARPins, designed ankyril repeat proteins; HER 2, human epidermal growth factor receptor 2; GNPs, gold nanoparticles; PTT, photothermal therapy; SK-BR-3, human breast adenocarcinoma cells; CHO, chinese hamster ovary cells; MD, molecular dynamics; AFM, atomic force microscopy; FITC, fluorescein isothiocyanate.

REFERENCES

1. Huang, H., Jain, P. K., El-Sayed, I. H. a,nd El-Sayed, M. A. (2008) Plasmonic Photothermal Therapy (PPTT) Using Gold Nanoparticles. *Lasers Med. Sci. 23*, 217–228.

2. Huang, X., and El-Sayed, M .A. (2010) Gold Nanoparticles: Optical Properties and Implementations in Cancer Diagnosis and Photothermal Therapy. *J. Adv. Res. 1*, 13–28.

3. Lucky, S. S., Soo, K. C., and Zhang, Y. (2015) Nanoparticles in Photodynamic Therapy. *Chem. Rev.*, *115*, 1990−2042.

4. Grebenik, E.A., Kostyuk, A.B., and Deyev, S.M. (2016) Upconversion Nanoparticles and Their Hybrid Assemblies for Biomedical Applications. *Russ. Chem. Rev. 85*, 1277–1296.

5. Govorov, A. O., and Richardson, H. H. (2007) Generating Heat with Metal Nanoparticles. *Nanotoday 2*, 30-38.

6. Verderio, P., Avvakumova, S., Alessio, G., Bellini, M., Colombo, M., Galbiati, E., Mazzucchelli, S., Avila, J. P., Santini, B., and Prosperi, D. (2004) Delivering Colloidal Nanoparticles to Mammalian Cells: a Nano–Bio Interface Perspective. *Adv. Healthcare Mater*. *3*, 957–976.

7. Deyev, S. M., Lebedenko, E. N., Petrovskaya, L. E., Dolgikh, D. A., Gabibov, A. G., and Kirpichnikov, M. P. (2015) Man-Made Antibodies And Immunoconjugates with Desired Properties: Function Optimization Using Structural Engineering. *Russ. Chem. Rev. 84*, 1–26.

8. Yan, Y., Such, G. K., Johnston, A. P. R., Best J. P., and Caruso F. (2012) Engineering Particles for Therapeutic Delivery: Prospects and Challenges. *ACS Nano 6*, 3663–3669.

9. Giljohann, D. A., Seferos, D. S., Daniel, W. L., Massich, M. D., Patel, P. C., and Mirkin, C. A. (2010) Gold Nanoparticles for Biology And Medicine. *Angew. Chem. Int. Ed. 49*, 3280 – 3294.

10. Nazarenus, M., Zhang, Q., Soliman, M. G., del Pino, P., Pelaz, B., Carregal-Romero, S., Rejman, J., Rothen-Rutishauser, B., Clift, M. J. D., Zellner, R., et. al. (2014) *in vitro* Interaction of Nanoparticles with Mammalian Cells: What Have we Learned Thus Far? *Beilstein J. Nanotechnol. 5*, 1477–1490.

11. Avvakumova, S., Colombo, M., Tortora, P., and Prosperi, D. (2014) Biotechnological Approaches Toward Nanoparticle Biofunctionalization. *Trends Biotechnol. 32*, 11-20.

12. Occhipinti, E., Verderio, P., Natalello, A., Galbiati, E., Colombo, M., Mazzucchelli, S.; Salvade, A., Tortora, P., Dogliaa, S. M., and Prosperi, D. (2011) Investigating the Structural Biofunctionality of Antibodies Conjugated to Magnetic Nanoparticles. *Nanoscale 3*, 387–390.

13. Binz, H. K., Amstutz, P., Kohl, A., Stumpp, M. T., Briand, C., Forrer, P., Grütter, M. G., and Plückthun A. (2004) High-Affinity Binders Selected from Designed Ankyrin Repeat Protein Libraries. *Nat. Biotechnol. 22*, 575–582.

14. Jost, C., Schilling, J., Tamaskovic, R., Schwill, M., Honegger, A., and Plückthun, A. (2013) Structural Basis for Eliciting a Cytotoxic Effect in HER2-Overexpressing Cancer Cells Via Binding to the Extracellular Domain of HER2. *Structure 21*, 1979–1991.

15. Tamaskovic, R., Simon, M., Stefan, N., Schwill, M., and Plückthun, A. (2012) Designed Ankyrin Repeat Proteins (Darpins): from Research to Therapy. *Meth. Enzymol. 503*, 101–134.

16. Verdurmen, W. P. R., Luginbühl, M., Honegger, A., and Plückthun, A. (2015) Efficient Cell-Specific Uptake of Binding Proteins into the Cytoplasm Through Engineered Modular Transport Systems. *J. Control. Release 200*, 13–22.

17. Steiner, D., Forrer, P., and Plückthun, A. (2008) Efficient Selection of Darpins with Sub-Nanomolar Affinities Using SRP Phage Display. *J. Mol. Biol. 382*, 1211–1227.

18. Martin-Killias, P., Stefan, N., Rothschild, S., Plückthun A., and Zangemeister-Wittke, U. (2011) A Novel Fusion Toxin Derived from an Epcam-Specific Designed Ankyrin Repeat Protein Has Potent Antitumor Activity. *Clin. Cancer Res. 17*, 100–110.

19. Proshkina, G., Shilova, O., Ryabova, A., Stremovskiy, O., and Deyev S. (2015) A New Anticancer Toxin Based on HER2/Neu-Specific Darpin and Photoactive Flavoprotein Minisog. *Biochimie 118*, 116–122.

20. Sokolova, E., Proshkina, G., Kutova, O., Shilova, O., Ryabova, A., Schulga, A., Stremovskiy, O., Zdobnova, T., Balalaeva, I., and Deyev S. (2016) Recombinant Targeted Toxin Based on HER2-Specific Darpin Possesses a Strong Selective Cytotoxic Effect *in vitro* and a Potent Antitumor Activity *in vivo*. *J. Control. Release 233*, 48–56.

21. Gebauer, S., Malissek, M., Simon, S., Knauer, S. K., Maskos, M., Stauber, R. H., Peukert, W., and Treuel, L. (2012) Impact of the Nanoparticle−Protein Corona on Colloidal Stability and Protein Structure. *Langmuir 28*, 9673−9679.

22. del Pino, P., Pelaz, B., Zhang, Q., Maffre, P., Nienhaus, G. U., and Parak W. J. (2014) Protein Corona Formation Around Nanoparticles – from the Past to the Future. *Mater. Horiz. 1*, 301–313.

23. Lynch, I., and Dawson, K. A. (2008) Protein-Nanoparticle Interactions. *Nano Today 3*, 40–47.

24. Zikich, D., Borovok, N., Molotsky, T., and Kotlyar, A. (2010) Synthesis and AFM Characterization of Poly(dG)-Poly(dC)-Gold Nanoparticle Conjugates. *Bioconjugate Chem. 21*, 544–547.

25. Jana, N. R., Gearheart, L., and Murphy, C. J. (2001) Seeding Growth for Size Control of 5−40 nm Diameter Gold Nanoparticles. *Langmuir 17*, 6782−6786.

26. Liu, X., Atwater, M., Wang, J., and Huo, Q. (2007) Extinction Coefficient of Gold Nanoparticles with Different Sizes and Different Capping Ligands. *Colloids and Surfaces B: Biointerfaces 58*, 3–7.

27. Mironova, K. E., Chernykh, O. N., Ryabova, A. V., Stremovskiy, O. A., Proshkina, G. M., and Deyev, S. M. (2014) Highly Specific Hybrid Protein Darpin-Mcherry for Fluorescent

Visualization of Cells Overexpressing Tumor Marker HER2/neu. *Biochemistry (Mosc.) 79*, 1391–1396.

28. Berman, H. M., Westbrook, J., Feng, Z., Gilliland, G., Bhat, T. N., Weissig, H., Shindyalov, I. N., and Bourne, P. E. (2000) The Protein Data Bank. *Nucleic Acids Res*. *28*, 235-242.

29. Tavanti F., Pedone, A., and Menziani, M. C. (2015) A Closer Look into the Ubiquitin Corona on Gold Nanoparticles by Computational Studies. *New J. Chem*. *39*, 2474–2482.

30. Tavanti, F., Pedone, A., and Menziani, M. C. (2015) Competitive Binding of Proteins to Gold Nanoparticles Disclosed by Molecular Dynamics Simulations. *J. Phys. Chem. C 119*, 22172–22180.

31. Brancolini, G., Kokh, D. B., Calzolai, L., Wade, R. C., and Corni, S. (2012) Docking of Ubiquitin to Gold Nanoparticles. *ACS Nano 6*, 9863–9878.

32. Hills, R. D., and Brooks, C. L. (2009) Insights from Coarse-Grained Gō Models for Protein Folding and Dynamics*. Int. J. Mol. Sci.*, *10*, 889–905.

33. Pincus, D. L, Cho, S. S, Hyeon, C, and Thirumalai, D. (2008) Minimal Models for Proteins and RNA from Folding to Function. *Prog. Mol. Biol. Transl. Sci*. *84*, 203-250.

34. Smith, W., and Forester, T. R., J. (1996) DL_POLY_2.0: a General-Purpose Parallel Molecular Dynamics Simulation Package. *Mol. Graph. 7855*, 136–141.

35. Horcas, I., Fernez, R., Gomez-Rodriguez, J. M., Colchero, J., Gomez-Herrero, J., and Baro, A. M. (2007) WSXM: a Software for Scanning Probe Microscopy and a Tool for Nanotechnology. *Rev. Sci. Instrum. 78*, 013705.

TOC

Synthesis, Characterization and Selective Delivery of DARPin-Gold Nanoparticle Conjugates to Cancer Cells

Sergey Deyev, Galina Proshkina, Anastasiya Ryabova, Francesco Tavanti, Maria Cristina Menziani, Gennady Eidelshtein, Gabriel Avishai, Alexander Kotlyar